Bulletin of Mathematical Biology (2006) 68: 99–130
DOI 10.1007/s11538-005-9066-z

ORIGINAL ARTICLE

Gene Expression Time Delays and Turing Pattern Formation Systems

E.A. Gaffney[a,*], N.A.M. Monk[b]

[a] *The School of Mathematics, The University of Birmingham, Edgbaston, Birmingham B15 2TT, UK*
[b] *Department of Computer Science, University of Sheffield, Sheffield S1 4DP, UK*

Received: 23 February 2005 / Accepted: 28 November 2005 / Published online: 23 March 2006

Abstract The incorporation of time delays can greatly affect the behaviour of partial differential equations and dynamical systems. In addition, there is evidence that time delays in gene expression due to transcription and translation play an important role in the dynamics of cellular systems. In this paper, we investigate the effects of incorporating gene expression time delays into a one-dimensional putative reaction diffusion pattern formation mechanism on both stationary domains and domains with spatially uniform exponential growth. While oscillatory behaviour is rare, we find that the time taken to initiate and stabilise patterns increases dramatically as the time delay is increased. In addition, we observe that on rapidly growing domains the time delay can induce a failure of the Turing instability which cannot be predicted by a naive linear analysis of the underlying equations about the homogeneous steady state. The dramatic lag in the induction of patterning, or even its complete absence on occasions, highlights the importance of considering explicit gene expression time delays in models for cellular reaction diffusion patterning.

Keywords Time delays · Reaction diffusion equations

1. Introduction

The development of multicellular organisms from a single fertilised egg cell is a complex spatio-temporal process. Central to the process is the ability of each cell formed during multiple rounds of cell division to adopt a state that is appropriate to its spatial and temporal position within the developmental process. The principal mechanism that allows cells with identical genetic material to adopt and maintain distinct states is differential gene expression. The degree to which each gene

*Corresponding author.
E-mail address: eag@for.mat.bham.ac.uk (E.A. Gaffney).

is expressed in a cell is controlled by a specific class of proteins (transcription factors). Successful development depends critically on the tight co-ordination in both space and time of gene expression in cells. This co-ordination is achieved by constant communication between cells over both short and long ranges. The signals exchanged, which can take many forms, have the capacity to influence gene expression in a way that is dependent on the states of both the sending and receiving cells. In this way, gene expression is co-ordinated in space and time so as to finally generate the stable pattern of differentiated cell types that is characteristic of each organism.

Recent experimental advances have provided detailed information on the molecular mechanisms that are involved in the establishment of patterns of gene expression in a number of model organisms. A key issue that remains difficult to address with current experimental techniques, however, is how local molecular interactions are coordinated in space and time. It is important to note that successful development depends not only on the generation of appropriate *spatial* patterns, but also on the *timing* of each pattern-forming event. Development proceeds at a well-defined (though temperature-dependent) rate for each organism, and this rate can be strikingly rapid. For example, the basic body plan of the zebrafish is established in under 24 h (Kimmel et al., 1995). When considering the overall tempo of a patterning event, it is essential to understand the timescales involved in the basic molecular processes that contribute to patterning. As stated above, patterning during development depends to a large extent on the regulation of gene expression.

Gene expression proceeds through a number of stages. First, a faithful transcript of the gene sequence is produced in the cell nucleus in the form of a linear polymeric ribonucleic acid (RNA) molecule. This primary transcript is then chemically processed in the nucleus. Specific sections of the transcript (introns) may be excised and the remaining sections (exons) spliced to produce a modified transcript known as messenger RNA (mRNA) that is then exported from the nucleus to the cytoplasm through pores in the nuclear membrane. In the cytoplasm, each mRNA can act as a template for protein synthesis. Complex molecular machinery translates the sequence of the mRNA molecule into the corresponding sequence of amino acids that constitutes a protein molecule. After further processing, the resulting protein molecules can then participate in cellular functions such as metabolism, regulation of transcription and intercellular signalling.

Given the complexity of these mechanisms, it is not surprising that a considerable delay can exist between a change in the primary events that regulate the level of expression of a gene (i.e. the rate at which primary transcripts of the gene are made) and the corresponding change in the rate of appearance of completed protein products. Furthermore, it is important to note that the processes of gene transcription and mRNA translation involve the production of long polymeric molecules by the sequential addition of monomers (typically in the range of thousands to millions per gene). Transcription and translation are thus genuine delay (rather than slow accumulation) processes: the output of the processes is a delayed function of the input. The magnitudes of transcriptional and translational delays clearly depend on the size of the genomic sequence of the gene in question; typical cumulative delays are of the order of a few tens of minutes, but can be as great as several hours (Tennyson et al., 1995).

Since the timescale of individual patterning events in development is of the same order of magnitude as these delays (particularly in fast-developing embryos such as zebrafish), it is important to explore the effects that time delays have on the form and tempo of pattern formation. However, the origin of these delays in the basic molecular events that underlie all cellular function make it very difficult to manipulate specific delays experimentally. Mathematical modelling provides a complementary approach to experimental manipulation, and provides an ideal setting in which to explore the effects of time delays in different mechanisms of pattern formation. In order to focus clearly on the effect of time delays, it is important to first consider simple models of pattern formation rather than detailed models that provide a more accurate description of real cellular events. The effects of delays on intracellular feedback circuits has been studied both generally (Mahaffy and Pao, 1984; Mahaffy, 1988) and, more recently, in relation to specific gene expression data (Monk, 2003). In the context of cellular pattern formation, delays have been proposed to play a central role in the generation of the spatially co-ordinated oscillations of gene expression underlying the formation of vertebrate somites (Lewis, 2003). Veflingstad et al. have used a model of Notch-mediated lateral inhibition to show that delays can have profound effects on the mode and tempo of cellular pattern formation (Veflingstad et al., 2005). In this study, we explore the effects of delays in a reaction diffusion model of pattern formation.

1.1. The reaction diffusion mechanism

The reaction diffusion mechanism is a particularly elegant means by which spatially heterogeneous patterns can form. Initially proposed by Turing (1952), this mechanism has since been explored in a large number of biological and chemical contexts, and has been experimentally verified for specific reacting chemical systems (Ouyang and Swinney, 1991). As a putative mechanism for biological pattern formation, it is commonly assumed that reacting and diffusing chemicals, referred to as morphogens, provide the source of spatial organisation, whereby concentration thresholds cue cell fate decisions, ultimately leading to global spatially heterogeneous patterns of cell state. This has been considered in numerous possible applications; early examples include animal coat markings (Murray, 1981, 1993), hair patterns in *Acetabularia* (Goodwin et al., 1985; Murray, 1993), dorso-ventral organisation of the embryonic sea urchin (Meinhardt, 1982), and stolon formation in marine hydroids (Meinhardt, 1982). These diverse models have many differences with regard to the assumptions concerning the interaction, production and decay of the morphogens. Nonetheless, it is assumed that the morphogens are transported by diffusion (and occasionally convection, as with marine hydroid stolon formation (Meinhardt, 1982)), and in particular that pattern is formed by short-range activation and long-range inhibition, as is characteristic of the eponymous Turing bifurcation. This bifurcation is typically shared among the many biologically motivated generalisations of the reaction diffusion mechanism such as the mechano-chemical models (Murray et al., 1983; Oster et al., 1983) which, in complete generality, can include effects due to, for example, cell convection, chemotaxis, haptotaxis and galvanotaxis (Murray, 1993).

These early models of pattern formation preceded the large amounts of recent molecular and genetic information currently being elucidated for many developmental and cellular pattern formation phenomena. As such, they were often considered to be simple representations of more complex underlying processes. For example, it was speculated that the short-range activation could be due to the autocatalysis of a slowly diffusing molecule, the self-induced release of a bound version of a poorly transported protein, or via a co-inhibitory mechanism (Meinhardt, 1982).

Since Turing's original proposal was made, it has become clear that a wide range of biological 'morphogens' direct differential cellular responses in development by inducing distinct levels of gene expression in responding cells (Tabata and Takei, 2004) at significant distances from their source (Vincent and Briscoe, 2001). However, while morphogens play significant roles in many pattern forming events during development, there is no definitive evidence for a set of Turing morphogens that generate pattern by undergoing a Turing bifurcation in a biological system. Nonetheless, there has been speculation that a Turing type mechanism may be involved in vertebrate limb development (Miura and Shiota, 2000; Glimm et al., 2004; Miura and Maini, 2004) and avian feather bud formation (Jung et al., 1998). In addition, a number of experiments have indicated that the secreted TGF-β proteins Nodal and Lefty behave as an activator-inhibitor reaction diffusion system in zebrafish mesendodermal induction (Chen and Schier, 2001, 2002; Branford and Yost, 2002, 2004; Solnica-Krezel, 2003; Chen and Shen, 2004).

Levels of gene expression are often assayed by *in situ* hybridisation, which allows the local concentration of specific mRNA transcripts to be visualised throughout a tissue, and thus provides an indication of the rates of transcription of target genes. It is this technique that has allowed the spatial distribution of putative morphogens to be visualised, for example during the formation of avian feather buds and zebrafish mesendoderm patterning. Thus, one can typically preclude the possibility raised in the modelling studies pre-dating such molecular data that short-range activation might be due to, for example, the self-induced release of a bound version of a protein.

Such observations are also important as they reveal an aspect to Turing's mechanism that has not been considered in biological pattern formation, at least outside the context of ecological systems. This aspect is the *time delay* associated with gene expression (see above). Since many of the putative morphogens that function during development are secreted proteins, they cannot regulate gene expression in target cells directly. Rather, they will typically bind to a cell-surface receptor and consequently modulate the activities of cytoplasmic proteins that transmit receptor-mediated signals to the nucleus (signal transduction). Signal transduction, and cytoplasmic processes required for the secretion from cells of further morphogens, can only increase the effective delay separating the receipt of a signal by a cell from any resulting changes in morphogen secretion by the cell. In the context of a reaction diffusion model, these delays will appear in the kinetic terms which represent the morphogen-regulated rates of morphogen production.

There have been a number of studies of reaction diffusion systems in the presence of time delays (Ruan, 1998; Boushaba and Ruan, 2001; Gourley and Ruan, 2002) in the context of nutrient recycling for plankton populations, with an overall

emphasis on the Turing instability. These studies show that a Turing instability is possible in such systems (Ruan, 1998; Boushaba and Ruan, 2001), but taking into account the diffusive transport of individuals during the time delay results in no Turing instability on a bounded domain (Gourley and Ruan, 2002). The Turing bifurcation has also been observed to fail for the modified Lengyel–Epstein two-variable model with time delays, used to simulate a delayed illumination feedback for the photosensitive chlorine dioxide–iodine–malonic acid (CDIMA) reaction (Li and Ji, 2004).

On surveying the possible effects of time delays on reaction diffusion models for pattern formation, one can immediately deduce that time delays do not affect the existence of steady states of the underlying equations. However, it is unclear whether they destabilise any steady state, to yield oscillatory solutions or whether they prevent a Turing instability from occurring. Equally importantly, in the context of development, it is also unclear whether time delays alter the rate at which the system may approach its large time asymptote. Changes in the time course of patterning, and in the nature of intermediate transients, can be of critical importance in a biological setting. Furthermore, it is important to note that in many developing systems domain growth occurs on roughly the same timescale as biological pattern formation (for example, Glimm et al., 2004). Thus, growth often constitutes an integral part of a pattern forming process and is known to exert a significant influence on the dynamics of the system in question (Arcuri and Murray, 1986; Kondo and Asai, 1995; Crampin et al., 1999, 2002; Glimm et al., 2004). Thus, the effects of domain growth are also considered in this paper.

In the following, we investigate the effects of gene expression time delays in an exemplar one dimensional, two component, reaction diffusion pattern formation model on both stationary domains and domains with spatially uniform exponential growth. Our ultimate aim is to determine whether or not the effects of gene expression time delays can substantially alter the behaviour of a putative cellular reaction diffusion patterning system.

2. Reaction diffusion model and linear theory

In this section, we introduce the exemplar reaction diffusion model that we will investigate, which has Schnakenberg kinetics, and we will briefly investigate the linear behaviour of perturbations from the homogeneous steady state. We take this opportunity to inform the reader that a summary table of all variables and parameters, excluding those introduced in the appendices, can be found in Appendix B.2.

2.1. Schnakenberg kinetics

There is not, as yet, a cellular pattern formation system fully characterised in terms of reacting and diffusing molecular components. Thus any cellular pattern formation reaction diffusion model ultimately speculates on the details of the

interactions for its various constituents. However, a common feature of all such models is the short-range activation and the long-range inhibition (Murray, 1993; Meinhardt, 1982). Thus, we here consider a model with Schnakenberg kinetics, which is the simplest reaction diffusion pattern formation system that has such an interpretation (p. 376–379, Murray, 1993).

For a suitable non-dimensionalisation, the Schnakenberg reaction diffusion equations, in the absence of domain growth and time delays, can be written in the form

$$\frac{\partial a}{\partial t} = \frac{D}{\lambda L_0^2}\frac{\partial^2 a}{\partial x^2} + p - ab^2, \qquad \frac{\partial b}{\partial t} = \frac{\epsilon^2 D}{\lambda L_0^2}\frac{\partial^2 b}{\partial x^2} + q - b + ab^2. \tag{1}$$

Here b is the concentration of the activator, a is the concentration of the inhibitor, $D > 0$ is the dimensional diffusivity of the inhibitor, $\lambda > 0$ is the dimensional decay rate of the activator and $L_0 > 0$ is the size of the physical domain. The decay rate λ is positive definite as we require activator decay to prevent an unphysical positive feedback in activator production. We have $x \in [0, 1]$, by the spatial rescaling, and p, q, ϵ are constant, with $p, q > 0$, $\epsilon \in (0, 1)$ and typically $\epsilon \ll 1$, which we will assume below at all times. Note that ϵ^2 is the ratio of the activator diffusion coefficient and the inhibitor diffusion coefficient. Neumann boundary conditions are the most appropriate for a biological domain in that one assumes the morphogens cannot escape at the domain edges; thus we have $\partial a/\partial x = \partial b/\partial x = 0$ at $x = 0, 1$.

With spatially uniform exponential growth of the one dimensional domain, the reaction diffusion equations can be written in the non-dimensionalised form (Crampin et al., 1999)

$$\frac{\partial a}{\partial t} = \frac{1}{\gamma(t)}\frac{\partial^2 a}{\partial x^2} + p - ab^2 - \frac{\delta}{2}a, \quad \frac{\partial b}{\partial t} = \frac{\epsilon^2}{\gamma(t)}\frac{\partial^2 b}{\partial x^2} + q - b + ab^2 - \frac{\delta}{2}b. \tag{2}$$

In the above $\gamma(t) = \lambda L^2(t)/D > 0$, where $\lambda > 0$ is the dimensional decay rate of the activator in the absence of domain growth, $D > 0$ is the dimensional diffusivity of the inhibitor and $L(t) > 0$ is the length of the biological domain, and thus positive definite. We have additionally defined $\delta = \dot{\gamma}/\gamma$ and, again, ϵ^2 is the ratio of diffusion coefficients. Note that the physical domain has been rescaled using a time-dependent transformation so that $x \in [0, 1]$; see Crampin et al. (1999) for more details. The Neumann boundary conditions are $\partial a/\partial x = \partial b/\partial x = 0$ at $x = 0, 1$.

2.1.1. The Turing instability

Let (a_*, b_*) denote the spatially homogeneous solution. For example, in the absence of growth, with $\delta = \dot{\gamma} = 0$, we have $(a_*, b_*) = (p/(p+q)^2, p+q)$.

Substitute the Fourier expansion

$$\begin{pmatrix} a \\ b \end{pmatrix} = \begin{pmatrix} a_* \\ b_* \end{pmatrix} + \eta \sum_{n=1,2,3,\ldots} \mathbf{A}_n(t)\cos(n\pi x) \tag{3}$$

into Eq. (2) with $\eta \ll 1$. Neglecting $O(\eta^2)$, we have

$$\frac{d\mathbf{A}_n}{dt} = -\frac{n^2\pi^2}{\gamma(t)}\begin{pmatrix} 1 & 0 \\ 0 & \epsilon^2 \end{pmatrix}\mathbf{A}_n + \begin{pmatrix} -b_*^2 - \delta/2 & -2a_*b_* \\ b_*^2 & 2a_*b_* - 1 - \delta/2 \end{pmatrix}\mathbf{A}_n \,. \tag{4}$$

Consider solutions of the form

$$\mathbf{A}_n(t) = \exp\left(\int_0^t ds\lambda_n(s)\right)\mathbf{B}_n, \tag{5}$$

where $\mathbf{B}_n$ is a constant vector. The function $\lambda_n(s)$ is readily solved for by substituting (5) into (4). For all other parameters fixed, the Turing bifurcation occurs on increasing γ from a sufficiently small value once $Re(\lambda_n)$ becomes positive for at least one value of n. In Appendix A.3 we show for $\epsilon^2 \ll 1$ that this occurs first for $n = 1$, with λ_1 real, once $\gamma > \gamma_{\text{crit}}$, where γ_{crit} is given by

$$\gamma_{\text{crit}} = \frac{2\pi^2\epsilon^2}{2a_*b_* - 1 - \frac{\delta}{2}}\left[1 - \frac{\epsilon^2\left(b_*^2 + \frac{\delta}{2}\right)}{2a_*b_* - 1 - \frac{\delta}{2}}\right]^{-1} \times \left[1 + \sqrt{1 - 4\epsilon^2\frac{b_*^2\left(1+\frac{\delta}{2}\right) + \frac{\delta}{2}\left(1+\frac{\delta}{2}\right) - \delta a_*b_*}{[2a_*b_* - 1 - \delta/2 - \epsilon^2(b_*^2 + \delta/2)]^2}}\right]^{-1}. \tag{6}$$

For typical parameter values considered in this paper we have

$$\gamma_{\text{crit}} = \frac{\pi^2\epsilon^2}{2a_*b_* - 1 - \delta/2}[1 + O(\epsilon^2)] = \frac{\pi^2\epsilon^2}{2a_*b_* - 1}[1 + O(\delta, \epsilon^2)].$$

We note that when there is no real, positive and bounded solution for γ_{crit}, as occurs with $2a_*b_* - 1 - \delta/2 \leq 0$ for example, we are in a region of parameter space where the Turing bifurcation does not occur. In the next sections we will focus on how a Turing bifurcation in a system lacking time delays is affected by the inclusion of time delays and thus restrict parameter values appropriately. Finally, note that one can immediately deduce that the non-autonomy does not significantly influence the location of the bifurcation, at least while $\delta \ll 1$.

2.2. Gene expression time delays

The autocatalytic production of the activator occurs via the non-linear terms $\pm ab^2$ in the above equations. This can be interpreted as a law of mass action balance for the reaction

$$A + 2B \rightarrow 3B,$$

where A, B denote the protein molecules whose concentrations are represented by a, b respectively. As illustrated previously, it is reasonable to assume that activator autocatalysis in the reaction diffusion mechanism occurs via gene expression. Such

a production mechanism would have to be subject to gene expression time delays, which are very roughly estimated to be in the range of 10 min to a few hours (Lewis, 2003).

In what follows, the timescale is taken to be the reciprocal of the decay rate of the activator. With a suitable scaling of the activator and inhibitor concentrations, the Schnakenberg reaction diffusion equations on a domain with spatially uniform exponential growth and a simple, non-distributed, gene expression time delay, can be written in the form

$$\begin{aligned}\frac{\partial a}{\partial t}+\frac{\partial}{\partial y}(ua) &= \frac{D}{\lambda}\frac{\partial^2 a}{\partial y^2}+p-a(y,t)b^2(y,t),\\ \frac{\partial b}{\partial t}+\frac{\partial}{\partial y}(ub) &= \frac{\epsilon^2 D}{\lambda}\frac{\partial^2 b}{\partial y^2}+q-b-2a(y,t)b^2(y,t)\\ &\quad +3a(y_\tau,t-\tau)b^2(y_\tau,t-\tau).\end{aligned} \tag{7}$$

As with Eq. (1), D is the dimensional diffusivity of the inhibitor, λ is the dimensional decay rate of the activator in the absence of domain growth and ϵ^2 is the ratio of diffusion coefficients. In addition, u is the velocity field of the domain growth and $y\in[0,L(t)]$, where $L(t)>0$ is the domain length. In what follows, we will restrict ourselves to considering uniform exponential growth

$$L(t)=L_0\,\mathrm{e}^{\delta t/2},\quad L_0>0.$$

We also have $t>\tau$, with τ denoting the gene expression time delay, and $y_\tau \stackrel{\text{def}}{=} Y_y(s=t-\tau)$, where $Y_y(s)$ is the solution of the characteristic equation

$$\frac{\mathrm{d}Y_y}{\mathrm{d}s}(s)=u(Y,s),\quad Y_y(s=t)=y.$$

Thus, Eq. (7) represents

$$A+2B$$

binding at a cell surface receptor at location (y,t), followed by signal transduction, regulated gene expression, and the subsequent release of $3B$ protein molecules after a gene expression time delay of τ. However, in this period, the cells are moved by the underlying domain growth velocity field u and hence at the location (y,t) the amount of B released is governed by events at location $(y_\tau,t-\tau)$. Note that *intra*cellular events are not considered to be subject to diffusion, as the *intra*cellular medium is not free to diffuse into the *extra*cellular medium.

Hence, we must only consider the effects of convection by the underlying domain growth velocity field in considering the delayed term, rather than considering both convection and diffusion. One might consider different kinetics with, for example, the three B molecules each being released at different times during the interval $[t-\tau,t]$. We will briefly address the issue of different kinetics in the discussion at the end of this paper.

With uniform exponential growth, $L(t) = L_0\,\mathrm{e}^{\delta t/2}$, we have (Crampin et al., 1999)

$$u(y,t) = y\frac{\dot{L}(t)}{L(t)} = \delta y/2.$$

Substituting this in the above equations yields $y_\tau = y\,\mathrm{e}^{-\tau\delta/2}$, and rescaling the spatial coordinate via $(x,t) = (y/L(t),t)$, yields the following non-dimensionalised equations

$$\begin{aligned}\frac{\partial a}{\partial t} &= \frac{1}{\gamma(t)}\frac{\partial^2 a}{\partial^2 x} + p - \frac{\delta}{2}a - a(x,t)b^2(x,t)\\ \frac{\partial b}{\partial t} &= \frac{\epsilon^2}{\gamma(t)}\frac{\partial^2 b}{\partial x^2} + q - b - \frac{\delta}{2}b - 2a(x,t)b^2(x,t)\\ &\quad + 3a(x,t-\tau)b^2(x,t-\tau).\end{aligned} \tag{8}$$

In the above equations $x \in [0,1]$ and $\gamma(t) = \lambda L_0^2\,\mathrm{e}^{\delta t}/D$. Note that the spatial nonlocality in Eq. (7) is no longer present. In addition, setting $\tau = 0$ in the above equations, one recovers Eq. (2).

2.2.1. The Turing instability revisited

With (a_*, b_*) again denoting the spatial homogeneous solution, substitute (3) into (8). Neglecting $\mathrm{O}(\eta^2)$ we have

$$\begin{aligned}\frac{\mathrm{d}\mathbf{A}_n}{\mathrm{d}t} &= -\frac{n^2\pi^2}{\gamma(t)}\begin{pmatrix}1 & 0\\ 0 & \epsilon^2\end{pmatrix}\mathbf{A}_n(t) + \begin{pmatrix}-b_*^2 - \delta/2 & -2a_*b_*\\ -2b_*^2 & -4a_*b_* - 1 - \delta/2\end{pmatrix}\mathbf{A}_n(t)\\ &\quad + \begin{pmatrix}0 & 0\\ 3b_*^2 & 6a_*b_*\end{pmatrix}\mathbf{A}_n(t-\tau) \stackrel{\text{def}}{=} -\frac{n^2\pi^2}{\gamma(t)}\begin{pmatrix}1 & 0\\ 0 & \epsilon^2\end{pmatrix}\mathbf{A}_n(t)\\ &\quad + \mathbf{P}\mathbf{A}_n(t) + \mathbf{Q}\mathbf{A}_n(t-\tau)\,.\end{aligned} \tag{9}$$

For no domain growth, one can consider γ as a bifurcation parameter. One can show, for $\epsilon \ll 1$, that there are no oscillations at the critical value of γ, i.e. γ_{crit}. This value corresponds to the bifurcation where Eq. (9) first exhibits a non-negative growth rate for $\mathbf{A}_n$, on increasing γ from a sufficiently small value, for any positive integer n. See Appendix A.3 for further details, where we additionally show that Eq. (6) also gives γ_{crit} for non-zero time delays in the absence of domain growth.

For time dependent γ, a linear analysis is not possible with standard techniques and hence we proceed numerically. The modulus of the first component of $\mathbf{A}_{n=1}$ is plotted for Eq. (9) in Fig. 1 with a selection of growth rates and time delays for a typical set of parameter values. These plots are representative. Many parameters and initial conditions have been considered and the comments made below apply generally; further results can also be found in Appendix A.1.

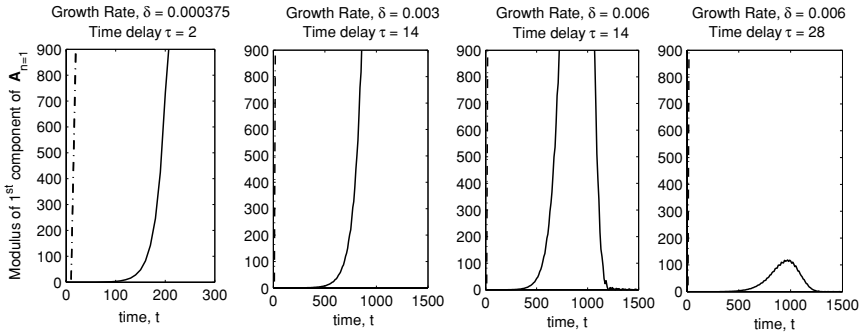

Fig. 1 Sample solutions for the modulus of the first component of $\mathbf{A}_{n=1}$ as governed by Eq. (9). *Solid lines* correspond to the values of the time delay and growth rate specified above each graph. *Dashed lines* correspond to the growth rates specified, but with zero time delay. The *solid line* in the third plot from the left peaks at an amplitude of ∼3500. The *solid line* in the two left-hand plots and the *dashed lines* grow indefinitely as time increases. In the above plots time is non-dimensionalised with respect to the inverse of the decay rate of the activator, λ^{-1}, while $n = 1$, $p = 0.9, q = 0.1, \epsilon^2 = 0.001, \gamma(t = 0) = 0.05$ and the initial conditions are $\mathbf{A}_{n=1} = (0.95, 1.05)$ for $t \in [0, \tau]$.

Note, firstly, the gene expression time delays do not induce oscillations in the linearised equations but they do drastically increase the time it takes for the system to move away from the homogeneous steady state. Furthermore, we see in the right-hand plots of Fig. 1 that the modulus of the first component of $\mathbf{A}_{n=1}$ increases at early time, followed by a peak, prior to an eventual decay back to O(1) values or less. In Appendix A.1 we observe that the large time asymptotes of the components of $\mathbf{A}_{n=1}$ always decay to O(1) values or less for sufficiently large $\tau\delta$. One cannot rely on naive instability arguments, where the dynamics are only considered near the homogeneous steady state, under such circumstances. For example, determining if the components of $\mathbf{A}_{n=1}$ initially move away from the homogeneous steady state is insufficient as it is not clear if this instigates an instability given that the large time asymptotes for the components of $\mathbf{A}_{n=1}$ could decay to O(1) values or smaller. The question of whether pattern actually forms depends on whether the size of the components of $\mathbf{A}_{n=1}$, and the value of η, are sufficient to allow the non-linear dynamics of the full Eqs. (8) to take hold and instigate a pattern. Ultimately, this depends on the full non-linear dynamics of the system and is not easily answered analytically. Thus, noting these limitations of a linear analysis, we will proceed to investigate the full non-linear equations, rather than investigate the linear equations further for $\tau\delta > 0$.

3. The non-linear, non-autonomous model

In the following section we present some representative parameter values and initial conditions required for detailed numerical simulations of the time delayed

Table 1 A reference set of parameter estimates for Eq. (8), used for Figs. 4 and 5. The timescale, as previously, is taken to be $1/\lambda$. Thus, the exponential domain growth rate, governed by $\delta/2$, corresponds to a dimensional domain doubling time of 2.0 days (2SF). The final time, T, corresponds to a dimensional value of 15.5 days (3SF). The gene expression time delay, τ, is given in terms of the parameter τ_0. This is typically the smallest time delay considered and is equivalent to a dimensional time delay of 12.0 min (3SF) for the choice of timescale. For these parameters $\gamma_{\text{crit}} > \gamma(t = 0)$ so that the homogeneous steady state is initially stable, though domain growth will eventually destabilise the system.

Parameter	Value
Diffusivity of the inhibitor (D, $\text{cm}^2\,\text{s}^{-1}$)	10^{-6}
Decay rate of the activator (λ, min^{-1})	1/3.1
Rate of exponential domain growth ($\delta = \dot{\gamma}/\gamma$)	0.0015
Non-dimensionalised base rate production	
Inhibitor (p)	0.90
Activator (q)	0.10
Ratio of diffusion coefficient (ϵ^2)	0.0010
Ratio of gene expression time delay to representative small time delay (τ/τ_0)	$\tau/\tau_0 \in \{0.0, 1.0, 2.0, 4.0, 8.0, 16.0\}$
Time (t)	$t \in [0, T = 7190]$
Representative small time delay (τ_0, min)	3.875
Initial value of γ ($\gamma(t = 0)$)	5.0×10^{-3}

reaction diffusion system given by Eq. (8) for both stationary domains and spatially uniform exponential domain growth.

3.1. Reference parameter values

In Table 1, we specify reference parameter values for a number of the simulations. The domain growth is uniform and exponential while the dimensional gene expression time delay is between 12 min and 3.2 h, which encompasses estimates for this parameter (Lewis, 2003). In Table 2, we have parameters associated with

Table 2 A reference set of parameter estimates for Eq. (8) in the absence of domain growth, used for Fig. 3. For these parameters, $\gamma_{\text{crit}} = 0.0124 < \gamma(t = 0)$, so that we are in the regime where the Turing instability will occur. As previously, the timescale is taken to be $1/\lambda$.

Parameter	Value
Diffusivity of the inhibitor (D, $\text{cm}^2\,\text{s}^{-1}$)	10^{-6}
Decay rate of the activator (λ, min^{-1})	1/3.1
Rate of exponential domain growth ($\delta = \dot{\gamma}/\gamma$)	0.00
Non-dimensionalised base rate production	
Inhibitor (p)	0.90
Activator (q)	0.10
Ratio of diffusion coefficient (ϵ^2)	0.0010
Ratio of gene expression time delay to representative small time delay (τ/τ_0)	$\tau/\tau_0 \in \{0.0, 1.0, 2.0, 4.0, 8.0, 16.0\}$
Representative small time delay (τ_0, min)	3.875
Initial value of γ ($\gamma(t = 0)$)	5.0×10^{-2}

no domain growth. Further, tables of representative parameter values used for the simulations below, which have differing growth rates (δ) and activator diffusivities ($\epsilon^2 D$), are listed in Tables B.1 and B.2 in Appendix B.2.

Given that no putative cellular reaction system has been completely determined in terms of its molecular constituents, there are no definitive parameter estimates for the diffusivities, parameters governing the kinetics or the length of time over which the pattern formation mechanism is active. (There may nonetheless be bounds on these quantities.) We are therefore forced to consider plausible parameter estimates while recognising that the numerical simulations can only sample a subregion of parameter space. As we will indicate, the qualitative behaviour we find in this paper is typical, at least for regions of parameter space that we have sampled.

3.2. Initial conditions

As with standard Turing models of biological pattern formation, we consider initial conditions that are perturbations of the homogeneous steady state. Our initial conditions below are based on the functions $a_{\mathrm{IC}=1}(x)$, $b_{\mathrm{IC}=1}(x)$ which are plotted in Fig. 2; algebraic expressions for these plots can be found in Appendix B.1. We will also consider initial conditions constructed from the following

$$a_{\mathrm{IC}=2}(x) = a_{\mathrm{IC}=1}(1-x), \quad b_{\mathrm{IC}=2}(x) = b_{\mathrm{IC}=1}(1-x). \tag{10}$$

There are a number of points to note about these functions. Firstly, they are a perturbation of the homogeneous steady-state solution of Eq. (8) (providing $\delta \ll 1$, as is the case here). Secondly, they are consistent with the zero flux boundary conditions. Thirdly, reference to Appendix B.1 will reveal that the perturbations have been constructed from polynomials, so that they would excite a large number of Fourier modes once such modes become unstable as γ increases.

Typical choices of initial conditions we will use below are of the form

$$a(x,t) = a_{\mathrm{IC}=1}(x), \quad b(x,t) = b_{\mathrm{IC}=1}(x) \qquad t \in [0,\tau], \tag{11}$$

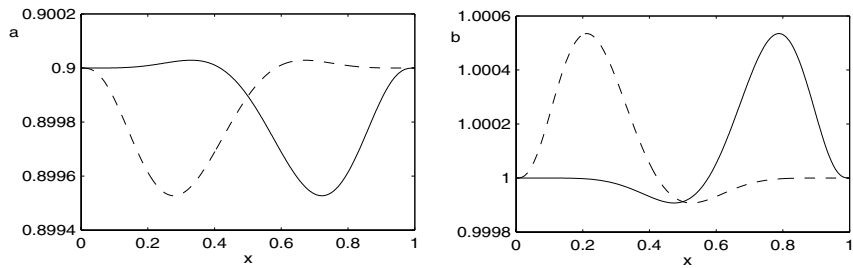

Fig. 2 The functions $a_{\mathrm{IC}=1}(x)$ and $b_{\mathrm{IC}=1}(x)$ are given by the *solid lines* in the above plot, while the functions $a_{\mathrm{IC}=2}(x)$ and $b_{\mathrm{IC}=2}(x)$ are given by the *dashed lines*. Note the vertical scales of these graphs; all of these functions are perturbations about $(a, b) = (0.9, 1.0)$.

or

$$a(x,t) = a_{\mathrm{IC}=2}(x), \quad b(x,t) = b_{\mathrm{IC}=2}(x) \qquad t \in [0,\tau], \tag{12}$$

where τ is the gene expression time delay. Another choice of initial conditions we will commonly use is

$$\begin{aligned} a(x,t) &= a_{\mathrm{IC}=1}(x)(1 + 0.0025\cos(\pi x)\,\cos(\pi t/(2\tau))) \qquad t \in [0,\tau], \\ b(x,t) &= b_{\mathrm{IC}=1}(x)(1 + 0.0025\cos(\pi x)\,\cos(\pi t/(2\tau))) \qquad t \in [0,\tau], \end{aligned} \tag{13}$$

and similarly for IC = 2. One should note that we have investigated the model for numerous other initial conditions in addition to those stipulated above, though perturbing the homogeneous steady state to a similar degree (not shown). The results presented below are representative of the behaviour observed in all our simulations.

4. Simulation results

In this section, we present results of numerical simulations of the time delayed reaction diffusion system given by Eq. (8) for both stationary domains and domains exhibiting uniform exponential growth. A standard, implicit, numerical method is used, though with time delays incorporated.

4.1. Gene expression time delays, with no domain growth

For the initial conditions given by Eqs. (11) and (12) and no domain growth, the main effect of the gene expression time delay is a large increase in the time required for the system to reach its long time asymptote. This is clearly illustrated in Fig. 3 where a gene expression time delay of τ_0, which corresponds to 12 min, induces an additional patterning lag of roughly $60\tau_0$. Similar observations have been consistently observed for other parameter values and other initial conditions discussed in Section (3.2).

One should also note that the time delays do not induce oscillations in this system, as observed generally. Furthermore, the location of the activator maximum in the large time asymptote in general can depend on the details of the initial conditions. By 'maximum' note that we always mean the maximum on varying the spatial coordinate, for fixed time, rather than global maximum across all space and time. Analogous results for all of the above are also observed when $\epsilon^2 = 0.016$.

4.2. Gene expression time delays and spatially uniform exponential domain growth

In Figs. 4–6, we have a domain doubling time of 2 days while in Fig. 7 the domain doubling time is 8 days and it is 12 h in Fig. 8. In all these plots $\gamma(t=0) < \gamma_{\mathrm{crit}}$ and the initial conditions consist of perturbations about the homogeneous steady state, as detailed in the figure captions.

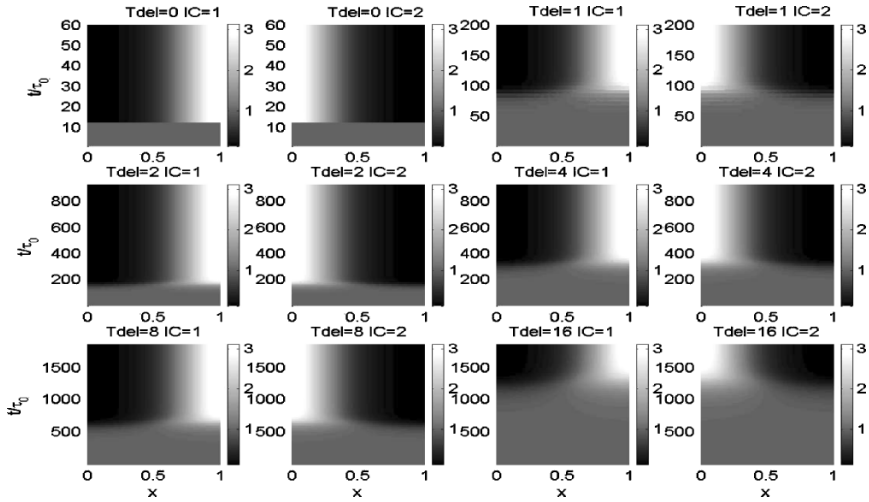

Fig. 3 In this figure, there are 12 greyscale plots for the activator, b, with the parameter values specified in Table 2. The horizontal axis represents the interval $x \in [0, 1]$, while the vertical axis represents t/τ_0, where τ_0 is the smallest gene expression time delay considered and is equivalent to a dimensional value of 12 min. The value of $b(x, t/\tau_0)$ is proportional to the greyscale at $(x, t/\tau_0)$ and can be determined using the greyscale bar to the right of each plot. The gene expression time delay for each plot is given by $\tau = T_{\text{del}}\tau_0$ where T_{del} is listed above each plot. The label IC = 1 corresponds to the initial conditions given by Eq. (11), while the label IC = 2 corresponds to the initial conditions specified in equation (12) on the time interval $[0, \tau]$. As mentioned in Section 1, it is typically assumed in pattern formation models that concentration thresholds in reacting and diffusing morphogens cue cell fate decisions. This is consistent with the prediction of a differential response in the above plots according to whether or not a cell is within a region of relatively high activator concentration. Similarly for the remaining figures in this paper.

4.2.1. Loss of robustness

By robustness, we mean a lack of sensitivity to small changes in the initial conditions. We can observe in Figs. 4–8 that in the absence of time delays, the activator pattern is independent of the initial conditions, at least once the central peak has formed. For $\tau\delta$ sufficiently large, a sensitivity to the initial conditions can be observed for $\epsilon^2 = 0.001$, as in Fig. 4 where the location of the activator peaks in general depends on the details of the initial conditions. For $\epsilon^2 = 0.016$ a loss of robustness can still occur (not shown) though it requires a fine tuning of the gene expression time delay to observe this.

4.2.2. The onset of patterning

One can readily make the important observation that the introduction of gene expression time delays leads to a substantial delay in the onset of patterning. This can be seen in more detail in Fig. 9 for a selection of parameter values. For example, in the third row of this figure, we have a magnification of runs which are governed by the parameters of Fig. 8. The initial conditions are those of Fig. 8 multiplied by a factor $(1 + 0.0025\cos(\pi x)\cos(t/2\tau))$. Note that $T_{\text{del}} = 0.5$ corresponds to a time delay of 6 min and for this time delay, the pattern initiates when $\gamma/\gamma_0 \sim 25$ while for no time delay the pattern initiates for $\gamma/\gamma_0 \sim 5$. Recall that γ scales

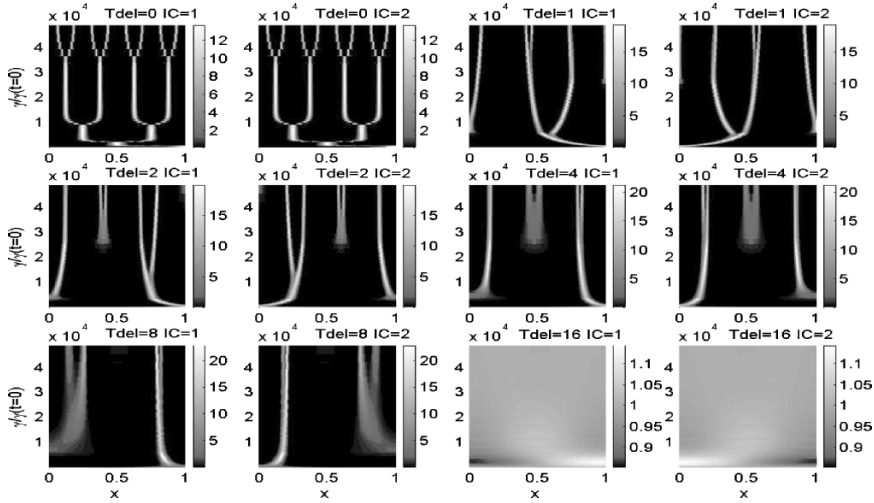

Fig. 4 With $\gamma(t=0) \stackrel{\text{def}}{=} \gamma_0$, note that γ/γ_0 is a monotonic function of time, t, and thus one can consider the activator concentration, b, as a function of $(x, \gamma/\gamma_0)$ rather than (x, t). In this figure, there are 12 greyscale plots of the activator, $b(x, \gamma/\gamma_0)$, for the parameter values specified in Table 1. Thus, the value of $b(x, \gamma/\gamma_0)$ is proportional to the greyscale at $(x, \gamma/\gamma_0)$ and can be determined using the greyscale bar to the right of each plot. The horizontal axis represents the interval $x \in [0, 1]$, while the vertical axis is $\gamma/\gamma(t=0)$, which is in the range $[1, 48000]$, corresponding to an increase in the domain length by a factor of approximately 220. We have $T_{\text{del}} \in \{0, 1, 2, 4, 8, 16\}$, which correspond to the values of τ specified in Table 1, i.e. $\tau = T_{\text{del}}\tau_0$, where τ_0 is the smallest gene expression time delay considered and is equivalent to a dimensional value of 12 min. We additionally have that IC = 1 corresponds to the initial conditions given by Eq. (11), while IC = 2 corresponds to the initial conditions specified by Eq. (12) on the time interval $[0, \tau]$. Analogous comments apply for the remaining figures.

with the square of the domain length. Thus, the effect of a 6 min time delay is to change the domain length at pattern initiation by a factor of $\sqrt{25/5} = 2.2$. Thus, the delay in the onset of patterning is roughly a domain doubling time, i.e. about 12 h. Analogous results are observed for other parameter values and initial conditions considered in both Fig. 9 and generally.

4.2.3. Highly irregular patterning and the failure of the Turing instability

The Turing bifurcation can be observed to fail. By this we specifically mean that an instability observed in the non-delayed system is absent due to the effects of a sufficiently large time delay. The Turing instability does not materialise in such cases even though the linear theory predicts that there is growth away from the homogeneous steady state, as illustrated in the right-hand plots of Fig. 1 for representative parameter values. Note that the reasons for why linear theory predictions of growth away from the homogeneous steady state do not necessarily predict an instability were discussed in Section 2.2.1.

The Turing instability fails in Fig. 4 for a gene expression time delay of $\tau = 16\tau_0$ and in an analogous manner, in Figs. 6 and 8. A highly irregular patterning is

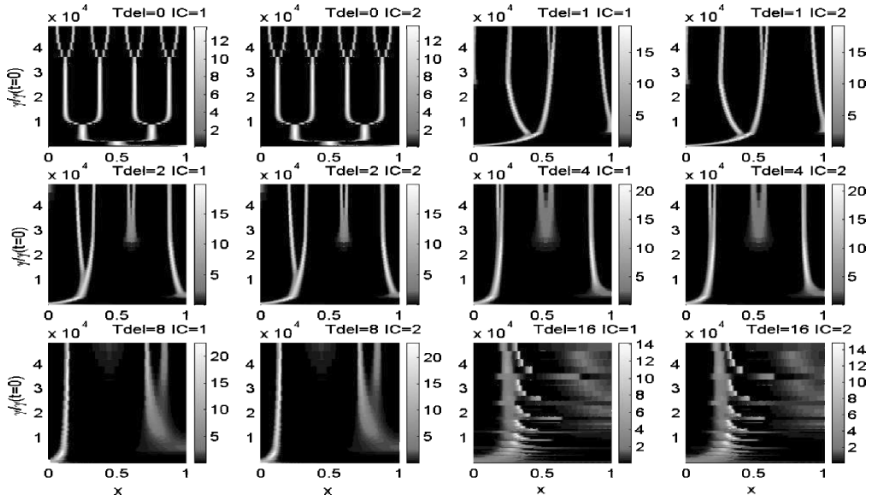

Fig. 5 Let $\gamma_0 \stackrel{\text{def}}{=} \gamma(t=0)$. In the above there are 12 grayscale plots of $b(x, \gamma/\gamma_0)$ for the parameter values specified in Table 1. As previously, the horizontal axis represents the interval $x \in [0, 1]$, while the vertical axis is $\gamma/\gamma(t=0)$. We have $T_{\text{del}} \in \{0, 1, 2, 4, 8, 16\}$, which correspond to the gene expression time delays specified in Table 1, namely $\tau = T_{\text{del}}\tau_0$, where τ_0 is the smallest gene expression time delay considered and is equivalent to a dimensional value of 12 min. We also have that IC = 1 and IC = 2 correspond to the initial conditions specified in Fig. 4, except that they are multiplied by the factor $(1 + 0.0025\cos(\pi x)\cos(t/(2\tau)))$, as specified in Eq. (13). Further details concerning the interpretation of these plots is provided in the caption for Fig. 4.

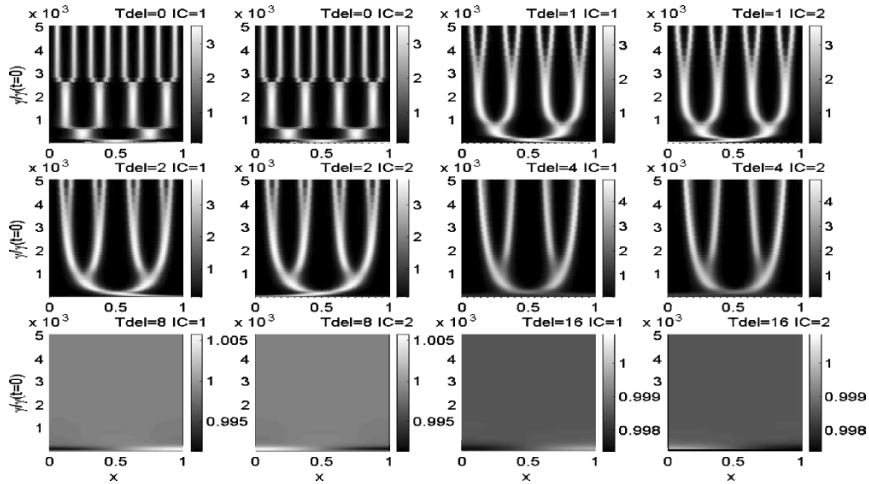

Fig. 6 Let $\gamma_0 \stackrel{\text{def}}{=} \gamma(t=0)$. In the above there are 12 grayscale plots of the activator, $b(x, \gamma/\gamma_0)$, with the parameter values and initial conditions specified for Fig. 4, except that $\epsilon^2 = 0.016$, $\gamma_0 = 0.08$ and the run duration is such that the domain increases in length by a factor of 70. Further details concerning the interpretation of these plots is provided in the caption for Fig. 4.

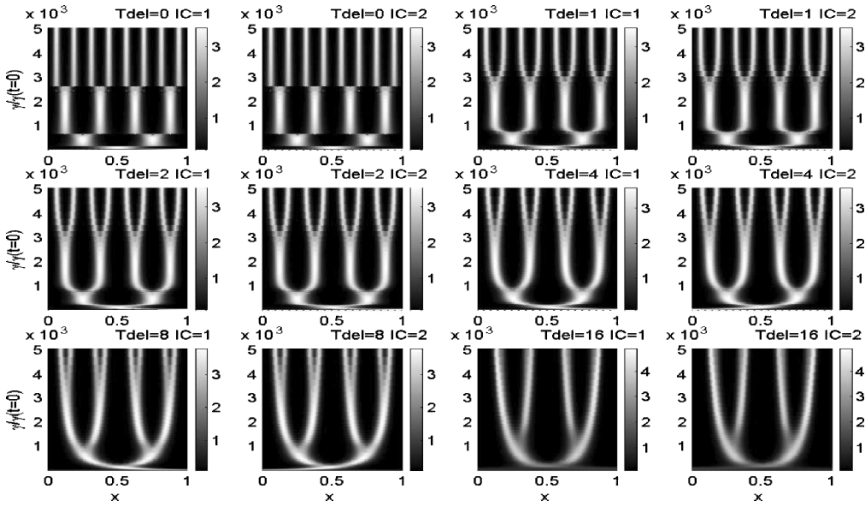

Fig. 7 As previously $\gamma(t=0) \stackrel{\text{def}}{=} \gamma_0$. In this figure there are 12 greyscale plots of the activator profile $b(x, \gamma/\gamma_0)$. The parameter values differ from Fig. 6 only in that the domain growth rate has been *reduced* by a factor of 4; the parameter values are listed in Table B.1 of Appendix B.2. The initial conditions are those used for Fig. 6 and are given by Eqs. (11) and (12) for IC = 1, IC = 2, respectively. Further details concerning the interpretation of these plots is provided in the caption for Fig. 4.

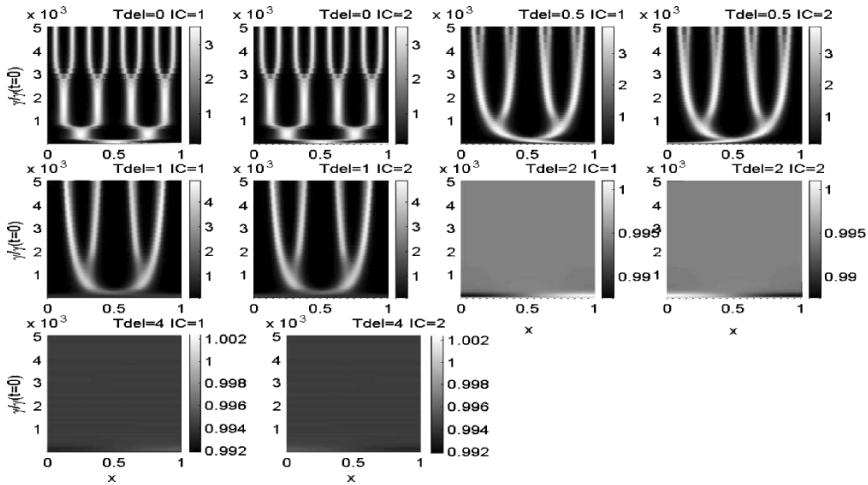

Fig. 8 Above there are 10 greyscale plots of the activator profile $b(x, \gamma/\gamma_0)$, where $\gamma(t=0) \stackrel{\text{def}}{=} \gamma_0$. The parameter values differ from Fig. 6 only in that the domain growth rate has been *increased* by a factor of 4 and a different selection of time delays in considered. These delays for each plot are given by $T_{\text{del}} \times \tau_0$, where T_{del} is specified above each plot and τ_0 corresponds to a dimensional gene expression time delay of 12 min for the non-dimensionalisation presented in Table 1. The parameter values are explicitly listed in Table B.2 of Appendix B.2. The initial conditions are those used for Fig. 6 and are given by Eqs. (11) and (12) for IC = 1, IC = 2 respectively. Further details concerning the interpretation of these plots is provided in the caption for Fig. 4.

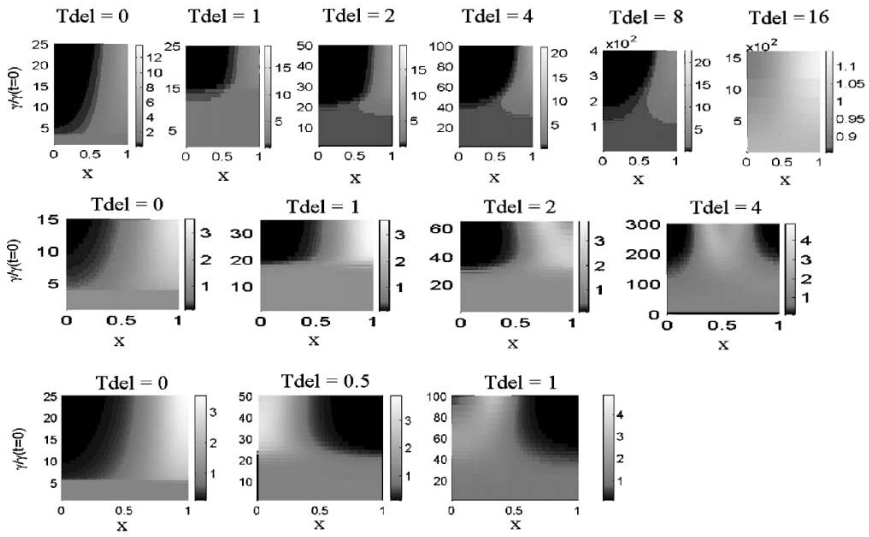

Fig. 9 In the first row, we have magnified the plots in Fig. 4 for IC = 1 and $T_{\text{del}} \in \{0, 1, 2, 4, 8, 16\}$. In particular, we have taken the vertical axis of each plot to be in a range of $\gamma/\gamma(t=0)$ which allows us to see when pattern formation first initiates. For example, in the left-hand plot of the first row, we have pattern first forming when $\gamma/\gamma(t=0) \sim 4$. In the plots on the first row, the gene expression time delay is $\tau = T_{\text{del}}\,\tau_0$, where τ_0 is the smallest time delay typically considered and corresponds to 12 min given the non-dimensionalisation presented in Table 1. Similar comments apply for the second and third rows. In the second row, the plots correspond to the early stages of the plots presented in Fig. 6 for IC = 1. In the third row, we have magnified the early stages of plots which have the same parameter values and IC = 1 initial conditions used in Fig. 8, except the initial conditions have been perturbed by the multiplicative factor $(1 + 0.0025\cos(\pi x)\,\cos(t/(2\tau)))$. See the text of Section 4.2.2 for further details.

observed in Fig. 5 for the largest time delay considered there. In Fig. 10, similar irregular behaviour can be observed when $\epsilon^2 = 0.016$ for the same initial conditions. One can observe that the precise onset of the failure of the Turing instability depends on the details of the initial conditions, by comparing Figs. 4 and 5. However, once highly irregular patterning is observed, small increases in the time delay subsequently result in a failure of the Turing instability. An illustration of this is given in Fig. 10 and is observed generally.

4.2.4. Oscillations

In general, oscillations of significant amplitude have not been commonly observed on the spatially growing domains for this model. The linear bifurcation analysis of Appendix A.3 also indicates that any growth away from the homogeneous steady state is, initially, non-oscillatory. Note though that oscillations can be present, as in Fig. 10, when the time delay is sufficiently large to induce the highly irregular behaviour discussed above, though some fine tuning of the time delay is required.

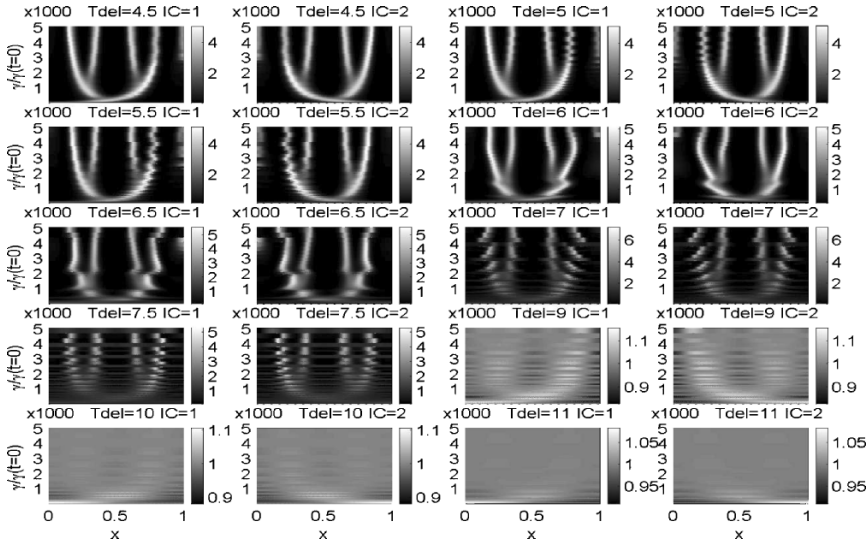

Fig. 10 In this figure there are 20 plots of the activator, b. The parameter values and initial conditions are the same as those used in Fig. 5 with the exception of the values for the gene expression time delay, $\epsilon^2 = 0.016$, $\gamma(t=0) = 0.08$ and the run duration. The latter is such that the domain length increases by a factor of 70. We have $T_{\text{del}} \in \{4.5, 5, 5.5, 6, 6.5, 7, 7.5, 9, 10, 11\}$, which gives the gene expression time delay $\tau = T_{\text{del}}\,\tau_0$. Here, we can see how the dynamics initially exhibits irregular behaviour as the gene expression time delay is raised, with the ensuing failure of the Turing instability as the time delay is increased further.

5. Discussion

In the following we are interested in assessing whether gene expression time delays can be neglected for the putative cellular pattern formation mechanism considered in this paper. We will consider both stationary domains and domains with uniform exponential growth. For the discussion below it will be useful to note that

$$\tau\delta = 2(\ln 2) \times \frac{\text{Gene expression time delay}}{\text{Domain doubling time}}\,.$$

This follows immediately on noting that $\delta/2$ is the exponential growth rate of the domain length $L(t)$ and hence the domain doubling time, t_{d}, is given by $t_{\text{d}} = (2\ln 2)/\delta$; dividing by the time delay, τ, gives the above after rearranging.

5.1. *No domain growth*

We firstly consider stationary domains and note that although time delays often induce oscillations in dynamical systems (see, for example, Veflingstad et al. (2005)), none are observed here. Thus, time delays need not invalidate reaction diffusion

models of pattern formation on stationary domains by inducing oscillatory (rather than stationary) patterns of activator and inhibitor concentrations.

We do, however, observe sensitivity of the final stationary pattern to the initial conditions, as illustrated by Fig. 3. Such sensitivity is a common and old criticism of reaction diffusion models (Bard and Lauder, 1974; Bunow et al., 1980) and is not specific to the presence of gene expression time delays. It can usually be eliminated in models that lack time delays by incorporating domain growth (Crampin et al., 1999) or by including the effects of an underlying asymmetry (Meinhardt, 1982; Page et al., 2005). In the absence of domain growth, which is considered below, we anticipate that the incorporation of an underlying asymmetry can enforce robustness in delay models as it does in non-delay models.

The most striking and important result of incorporating a gene expression time delay into our reaction diffusion model is that the times to the onset of patterning and to approach the large time asymptotic behaviour increase dramatically as the delay is increased. Thus, even for quite modest delays of 10 or 20 min, the time taken for the system to achieve pattern is increased by several hours. Such delays in the onset and/or stabilisation of pattern impose potentially severe constraints on the domain of applicability of reaction diffusion models that rely on regulated gene expression. In particular, in the context of embryonic development, where the timescale of pattern establishment is typically only a few hours and cells have limited time windows in which they are competent to respond to patterning cues (Kimmel et al., 1995), our results illustrate clearly the importance of considering gene expression time delays in proposed models of pattern formation. Since timing is of importance in all biological systems, it is also clear that any time delays existing in putative patterning mechanisms should not be neglected in general, as will be discussed in detail in the following sections.

5.2. Spatially uniform exponential domain growth

We proceed to consider spatially uniform exponential growth. It is interesting to observe the close similarity between the plots in Fig. 6 with $T_{\mathrm{del}} = 2$, 4 and the plots in Fig. 7 with $T_{\mathrm{del}} = 8$, 16. Similarly, for the plots in Fig. 8 with $T_{\mathrm{del}} = 0.5$, 1. The respective plots share the same value of $\tau\delta$ and initial conditions. This strongly indicates that the effect of the gene expression time delays and domain growth with regard to the failure of the Turing instability, the onset of irregular patterning or the eventual pattern formed, is governed by the parameter grouping $\tau\delta$. Further evidence of this is presented in Appendix A.2 and has been observed generally.

5.2.1. Loss of robustness

For sufficiently rapid domain doubling times, the presence of gene expression time delays can entail that the incorporation of domain growth is not sufficient to eliminate a sensitivity to the initial conditions, as seen in Fig. 4. This is in contrast to general conclusions arising in Crampin et al. (1999) when no time delays are present. However, we do not envisage this to be a severe problem for the reaction diffusion mechanism in virtually all of its applications, as we anticipate, but do not explicitly show here, that the effects of an underlying asymmetry can enforce

robustness (as in Meinhardt (1982)). In addition, the loss of robustness is no longer manifest, apart from with parameter fine tuning, when $\epsilon^2 = 0.016$. This additionally indicates that for larger values of ϵ^2, the loss of robustness is no longer an important issue.

5.2.2. The onset of patterning

As with no domain growth, we have the very important observation that small gene expression time delays induce a much larger time delay in the patterning onset and the time taken for the system to approach its large time asymptotic behaviour. Thus, in the presence of uniform exponential domain growth, we can also conclude that the patterning lag can be highly sensitive to the inclusion of time delays.

5.2.3. Highly irregular patterning and the failure of the Turing instability

All our simulations are consistent with the observation that once $\tau\delta$ is sufficiently large, the Turing instability fails, though the details of how large the time delay must be to prevent the Turing instability from occurring can depend on the initial conditions.

To place the above observation in context, we note that detailed simulations show that highly irregular behaviour or a Turing instability failure will occur once $\tau\delta > 1/30$ for $\epsilon^2 = 0.016$. Consider a gene expression time delay at the minimum estimate of 10 min (Lewis, 2003), which is probably the most appropriate estimate for a fast developmental process. For this time delay, and $\epsilon^2 = 0.016$, the domain doubling time has to be greater than 5 h, to ensure the Turing instability and regular patterning. We note that some developmental processes with Zebrafish for example occur with domain growth on significantly faster timescales (Kimmel et al., 1995).

From such observations, the failure of the Turing instability is typically outside the range of possible parameter values for the current model. However, irregular patterning or a Turing instability failure can occur if the domain is growing at a rate commensurate with the very fastest developmental processes. Thus, we have the observation that when modelling such processes, one should again explicitly justify the neglect of gene expression time delays if a Turing bifurcation is a possibility as, for the putative model here, it can make a substantial difference.

5.2.4. Oscillations

From our observations, oscillations can occur in parallel with highly irregular patterning with a careful choice of the time delay. However, the set of parameter values for which oscillations occur is observed to be a subset of the parameter space where regular patterning fails due to the occurrence of highly irregular behaviour or the failure of the Turing instability. Thus it is more important to investigate and delimit where the latter occur, as performed above.

5.2.5. Sensitivity to the details of the kinetics and other modelling assumptions

We note briefly that the non-dimensionalisation timescale, taken to be $\lambda^{-1} = 3.1$ min, can be changed without changing the key observations of this paper. For example, the failure of the Turing instability is governed by $\tau\delta$ which is independent of alternative timescales. Similarly, the size of the ratio of the gene

expression time delay to the additional lag in the patterning onset is independent of a temporal rescaling. Thus the key observations presented here are in fact valid for a family of dimensionalised parameter values, generated by altering the non-dimensionalisation timescale. We have also observed that the overall behaviour of the system with regard to the final pattern, the onset of irregular patterning and the failure of the Turing instability, is most strongly determined by the parameter grouping $\tau\delta$. Taking into account the results of Appendix A.2 this observation has held for an order of magnitude variation in each of ϵ^2, τ and δ. Similarly, the additional lag in the patterning onset has always been observed to be much greater than the gene expression time delay.

Nonetheless, we have still only sampled a fraction of parameter space. However, the fact we have not conducted an exhaustive search of parameter space should not be seen as a fundamental weakness of the paper. Here, our aim is to illustrate the effects of gene expression time delays, and to show that in general they cannot simply be dismissed for a representative selection of parameter values and initial conditions for a representative model.

Furthermore, most models incorporate pattern formation kinetics that are caricatures of more realistic kinetics, assuming these are even known. It is typically considered that such systems are effectively equivalent (e.g. p. 438, Murray (1993)). However, if this proves to be no longer true on incorporating gene expression time delays, then one has also to carefully justify the details of the choice of kinetics. This would typically require more information than is available for a given cellular pattern formation system. Under such circumstances, the presence of gene expression time delays would present a considerable obstacle for the determination of whether reaction diffusion pattern formation mechanisms are present in cellular contexts. This clearly merits further investigation.

6. Summary, conclusions and future work

We have motivated why, biologically, one needs to consider including gene expression time delays in the formulation of putative reaction diffusion models of cellular pattern formation processes. In turn, we have derived an exemplar model exhibiting this phenomenon utilising Schnakenberg kinetics on a fixed domain and on a domain which is uniformly growing at an exponential rate.

Our most important observation is that small gene expression time delays induce a large increase in the time required for the onset of pattern formation on both a fixed domain and for spatially uniform exponential domain growth.

Our study also demonstrates that, in the presence of such domain growth and gene expression time delays, a naive linear analysis that relies on determining whether there is an initial growth of perturbations about a steady state, is conceptually unreliable in predicting when a Turing instability occurs. In addition, on the growing domains considered, the behaviours observed in numerical simulations are governed by the ratio of the gene expression time delay to the domain doubling time. We observe the onset of highly irregular behaviour and/or a failure of the Turing instability once this ratio is sufficiently high. However, failure occurs only for the very fastest domain doubling times, at least for the exemplar model

considered here. Finally, we have seen that in the presence of gene expression time delays, pattern sensitivity to the initial conditions can occur, especially for very low ratios of activator to inhibitor diffusivities. However, we anticipate that this pattern sensitivity could be overcome by incorporating spatial asymmetry, as has been demonstrated for non-delayed systems.

The above observations do not rule out reaction diffusion as a putative pattern formation mechanism, whether on a stationary or uniformly growing spatial domain. However, when considering patterning events for which rapid establishment of pattern is critical, such as in the tissues of developing embryos, our results show that any putative time delays cannot be neglected in general without careful justification. In particular, our finding that time delays dramatically increase the time taken for the reaction diffusion system to initiate patterns imposes potentially severe constraints on the potential molecular details of any Turing system that might operate during developmental patterning.

In this paper, we have studied the effect of a single delay in a specific kinetic scheme. It would be interesting to extend this work to the case of multiple gene expression time delays, for non-exponential, non-uniform and reactant-controlled growth, and in higher spatial dimensions. Similarly, it would be interesting to consider the effects of gene expression time delays on alternative pattern formation models, such as those based on mechano-chemical mechanisms. In particular, we note that in the specific kinetics that we have studied, the time delay appears only in a positive feedback term of the activator equation. Previous work on diverse delay systems has shown that delays are most likely to induce oscillatory dynamics when they occur in negative feedback loops. Given that we have not found evidence for prominent oscillatory dynamics in our model, it would be of particular interest to explore alternative patterning mechanisms that incorporate delayed negative feedback terms. Finally, we note that we have only explored the effects of a discrete delay in this paper. Distributed delays provide a more realistic representation of gene expression mechanisms, and an exploration of the effects of distributed delays in a range of kinetic schemes would certainly be worthwhile. Such work is in progress.

A Appendices: supplementary information

A.1 Further results for the non-autonomous, time delayed, linear equations

Our starting point is Eq. (9) which governs the behaviour of $\mathbf{A}_n$ in Section 2.2.1, where we remarked that once $\tau\delta$ is sufficiently large, the components of $\mathbf{A}_{n=1}$ will peak before decaying to O(1) values or less for sufficiently large time. This can be observed in the two right-hand plots of Fig. 1. Here we illustrate, numerically, that this behaviour is commonplace. We solve the retarded Eq. (9) with $n = 1$, $p = 0.9$, $q = 0.1$, $\epsilon^2 = 0.001$, $\gamma(t = 0) = 0.05$, for a wide range of values for the exponential growth rate, δ, and the gene expression time delay, τ, with initial conditions $\mathbf{A}_{n=1} = (1.05, 0.95)$ for $t \in [0, \tau]$. Time is non-dimensionalised with respect to the inverse of the decay rate of the activator, denoted λ^{-1}, consistent with the scalings used in Section 2.2.1.

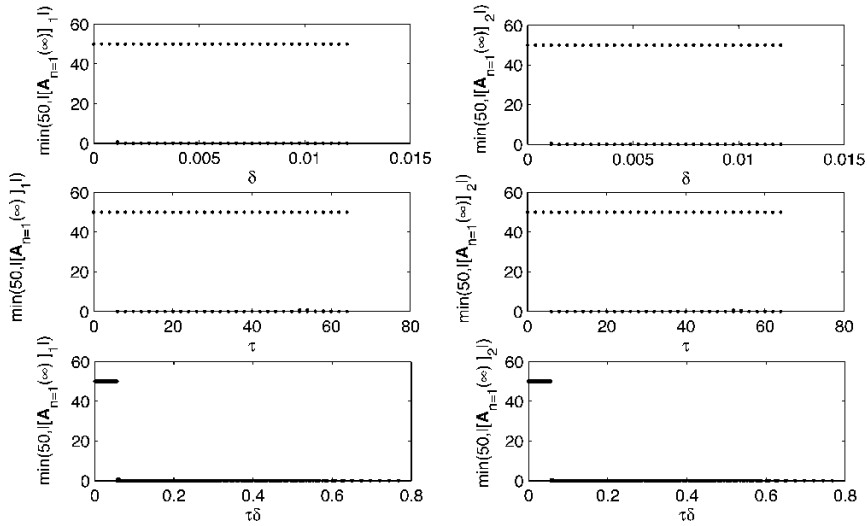

Fig. 11 The plots show $\min\{50, |[\mathbf{A}_{n=1}(\infty)]_1|\}$ and $\min\{50, |[\mathbf{A}_{n=1}(\infty)]_2|\}$. Note that $|[\mathbf{A}_{n=1}(\infty)]_i|$ denotes the modulus of the large time asymptote for the ith component of $\mathbf{A}_{n=1}$. See Appendix A.1 for further details and parameter values.

Let $|[\mathbf{A}_{n=1}(\infty)]_i|$, $i \in \{1, 2\}$, denote the large time asymptote of the modulus of the ith component of $\mathbf{A}_{n=1}$. We wish to observe when $|[\mathbf{A}_{n=1}(\infty)]_i|$ takes O(1) values or less and how this depends on the domain growth rate, δ, and the time delay τ. Given $|[\mathbf{A}_{n=1}(\infty)]_i|$ will be unbounded for certain choices of δ and τ we plot $\min(50, |[\mathbf{A}_{n=1}(\infty)]_1|)$, $\min(50, |[\mathbf{A}_{n=1}(\infty)]_2|)$. Hence, for example, if a plot has a value of 50, the large time asymptote is clearly not O(1) or less and we thus have sufficient information for our needs. In all our plots $\min(50, |[\mathbf{A}_{n=1}(\infty)]_1|)$ and $\min(50, |[\mathbf{A}_{n=1}(\infty)]_2|)$ are estimated numerically from the values of $\mathbf{A}_{n=1}$ at $t = 10^4\lambda^{-1}$ which, for the parameters of this paper, is a very long timescale.

We first plot $\min(50, |[\mathbf{A}_{n=1}(\infty)]_1|)$ and $\min(50, |[\mathbf{A}_{n=1}(\infty)]_2|)$ against δ in the upper row of Fig. 11. Each mark in these plots will typically correspond to more than one data point; for example, the marks for a given δ will generally correspond to numerous values of τ. From the third row of Fig. 11, we can clearly see that once $\tau\delta$ gets sufficiently large (> 0.057 approx.), the large time values of components of $\mathbf{A}_{n=1}$ are always O(1) or less. We have considered numerous other initial conditions which yield identical plots, while results with other parameter values, including changing ϵ^2 to 0.016, are analogous.

A.2 Further results: non-linear simulations

In Figs. 12 and 13 there are further additional results for $\epsilon^2 = 0.001$ with the same initial conditions as presented in Fig. 5. The plots are different from those in Fig. 5 only in that the domain growth rate is increased by a factor of four in Fig. 12 and decreased by a factor of four in Fig. 13. It is interesting to observe the similarity

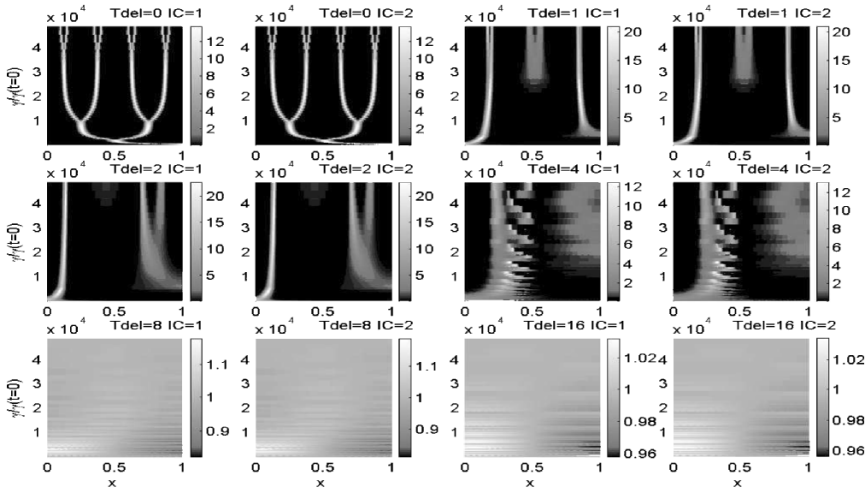

Fig. 12 As previously $\gamma(t=0) \stackrel{\text{def}}{=} \gamma_0$. There are 12 greyscale plots of the activator profile $b(x, \gamma/\gamma_0)$. The parameter values correspond to an *increase* in the exponential growth rate by a factor of 4 compared to the parameters in Table 1 and Fig. 5. All other parameters, the axes and the initial conditions are as specified in Fig. 5. The time delays for each plot are given by $T_{\text{del}} \times \tau_0$, where T_{del} is specified above each plot and τ_0 corresponds to a dimensional gene expression time delay of 12 min for the non-dimensionalisation presented in Table 1. Further details concerning the interpretation of these plots is provided in the caption for Fig. 4.

between the plots in Fig. 12 with $T_{\text{del}} = 1, 2, 4$ and the plots in Fig. 5 with $T_{\text{del}} = 4, 8, 16$. Also observe that plots in Fig. 5 with $T_{\text{del}} = 1, 2, 4$ are similar to plots with $T_{\text{del}} = 4$, 8, 16 in Fig. 13. This adds further evidence to the observation that the effect of the gene expression time delays with regard to the final pattern, and the onset of irregular patterning and the failure of the Turing instability, is governed by the parameter grouping $\tau\delta$.

A.3 A linear analysis of the time delayed equations

In this appendix we will perform a linear analysis of the time delayed equations close to the steady state. We assume $\epsilon^2 \ll 1$ and we will:

- prove that in the absence of domain growth, there are no oscillations for the linearised time delayed equations at the Turing bifurcation. This corresponds to the point where, treating γ as a bifurcation parameter, an instability is first induced by increasing γ from a sufficiently small value.
- derive Eq. (6) for (i) $\tau = 0,\ \delta \geq 0$ and (ii) $\delta = 0,\ \tau \geq 0$.

To proceed, let $p_{11}, p_{12}, \ldots, q_{21}, q_{22}$ denote the components of **P** and **Q** in Eq. (9). We have $q_{11} = q_{12} = 0$ and we will additionally assume the remaining of these parameters are of unit magnitude with $p_{22} + q_{22} > 0$, $q_{22} > 0$, as is the case for the kinetics used throughout this paper.

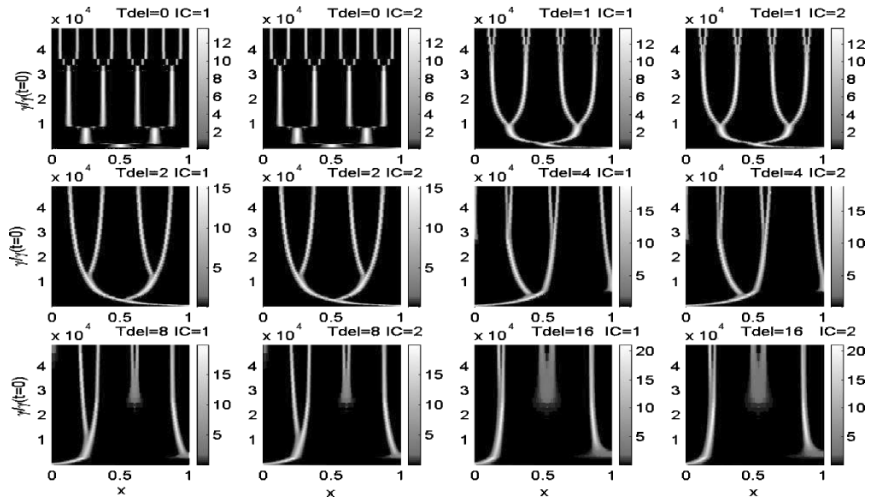

Fig. 13 There are 12 greyscale plots of the activator profile $b(x, \gamma/\gamma_0)$, where $\gamma(t=0) \stackrel{\text{def}}{=} \gamma_0$. The parameter values correspond to a *decrease* in the exponential growth rate by a factor of 4 compared to the parameters in Table 1 and Fig. 5. All other parameters, the axes and the initial conditions are as specified in Fig. 5. The time delays for each plot are given by $T_{\text{del}} \times \tau_0$, where T_{del} is specified above each plot and τ_0 corresponds to a dimensional gene expression time delay of 12 min for the non-dimensionalisation presented in Table 1. Further details concerning the interpretation of these plots is provided in the caption for Fig. 4.

A.3.1 No oscillations for the linearised time delayed equations at the Turing bifurcation

Substitute $\mathbf{A}_n(t) = \exp[\lambda_n t]\mathbf{B}_n$ into Eq. (9) for γ constant, $\delta = 0$ and $\tau > 0$. As with a standard linear instability analysis in the absence of delays, the λ_n are complex growth rates governing the behaviour of the linearised perturbations about the homogeneous steady state. The critical value of γ, denoted γ_{crit}, will correspond to where $\text{Re}(\lambda_n)$ first becomes zero on increasing γ, for any positive integer value of n. With $\text{Re}(\lambda_n) = 0$, $\text{Im}(\lambda_n) = \beta$ one can show that $\text{Re}(\lambda_n)$ first becomes zero on increasing γ for the smallest $\gamma_n(\beta, \tau)$, $n \in \mathbb{Z}^+$, $\beta \in \mathbb{R}$ satisfying *both*

$$\gamma_n(\beta, \tau) = \frac{2n^2\pi^2\epsilon^2}{A(\beta\tau) + \sqrt{A^2(\beta\tau) - \epsilon^2 B(\beta, \tau)}} \tag{A.1}$$

$$[\beta(1+\epsilon^2) + q_{22}\sin(\beta\tau)]\frac{n^2\pi^2}{\gamma_n(\beta,\ \tau)} \ = \ C(\beta, \tau) \tag{A.2}$$

where

$$\begin{aligned} A(\beta\tau) &\stackrel{\text{def}}{=} q_{22}\cos(\beta\tau) + p_{22} + \epsilon^2 p_{11} \\ B(\beta, \tau) &\stackrel{\text{def}}{=} 4\left[(p_{11}p_{22} - p_{12}p_{21}) + (p_{11}q_{22} - p_{12}q_{21})\cos(\beta\tau) - \beta q_{22}\sin(\beta\tau) - \beta^2\right] \\ C(\beta, \tau) &\stackrel{\text{def}}{=} p_{11}[\beta + q_{22}\sin(\beta\tau)] + \beta(p_{22} + q_{22}\cos(\beta\tau)) - p_{12}q_{21}\sin(\beta\tau). \end{aligned} \tag{A.3}$$

Clearly, the smallest value of γ corresponds to $n = 1$, and we take $n = 1$ below. Further note that $\beta = 0$ is consistent with Eq. (A.2) and, from Eq. (A.1), yields

$$\gamma_1(0,\tau) = \frac{2\pi^2\epsilon^2}{A(0) + \sqrt{A^2(0) - \epsilon^2 B(0,\tau)}} = \frac{\pi^2\epsilon^2}{A(0)}(1 + \mathrm{O}(\epsilon^2)) = \frac{\pi^2\epsilon^2}{p_{22} + q_{22}}(1 + \mathrm{O}(\epsilon^2)),$$

using the fact that $A(0)$, $B(0,\tau)$ are of unit magnitude.

We now seek other values of β which give consistent solutions of Eqs. (A.1) and (A.2) and which yield a smaller value of γ_1. For $|\beta| > 0$, we have by combining Eqs. (A.1) and (A.2) that

$$[\beta(1+\epsilon^2) + q_{22}\sin(\beta\tau)]\big[A(\beta\tau) + \sqrt{A^2(\beta\tau) - \epsilon^2 B(\beta,\tau)}\big]\frac{1}{2\epsilon^2} = C(\beta,\tau). \tag{A.4}$$

Firstly, suppose that $1 \gg \beta > 0$. Expanding the above, in terms of β yields

$$\frac{\beta}{\epsilon^2}(1 + q_{22}\tau + \mathrm{o}(1))(p_{22} + q_{22} + \mathrm{o}(1)) = \beta[p_{11} + q_{22}p_{11}\tau + p_{22} + q_{22} - p_{12}q_{22}\tau + \mathrm{o}(1)].$$

Noting that $q_{22} > 0$, $p_{22} + q_{22} > 0$ and of unit magnitude, it is impossible to balance the left and right hand sides for sufficiently small ϵ^2; thus we can note that there is no solution for $1 \gg |\beta| > 0$. Note that Eq. (A.4) can only be satisfied if $C(\beta,\tau) \gg 1$ or one of the bracketed terms on the left of this expression is much smaller than unity (or some combination of these possibilities). Further suppose that

$$|A(\beta\tau) + \sqrt{A^2(\beta\tau) - \epsilon^2 B(\beta,\tau)}| \ll 1.$$

This, combined with Eq. (A.1), entails that the resulting value of γ must be much larger than $\gamma_1(0,\tau)$. This therefore cannot yield the bifurcation point.

Suppose instead that $C(\beta,\tau) \sim \mathrm{O}(1/\epsilon^2)$. For a fixed gene expression time delay τ, and $\epsilon \ll 1$ sufficiently small, we ultimately require $\beta \sim \mathrm{O}(1/\epsilon^2)$. However, for $|\beta| \gg 1$, we have, from equation (A.2) that

$$|\gamma_1(\beta,\tau)| = \left|\frac{\pi^2(1 + \mathrm{O}(|\beta|^{-1}) + \mathrm{O}(\epsilon^2))}{p_{22} + p_{11} + q_{22}\cos(\beta\tau)}\right| \gg \gamma_1(0,\tau) \sim \mathrm{O}(\epsilon^2).$$

Thus, again, the resulting value of γ cannot correspond to the critical value of γ for sufficiently small ϵ.

Finally, suppose that $[\beta(1+\epsilon^2) + q_{22}\sin(\beta\tau)] \sim \mathrm{O}(\epsilon^2)$. For $\tau \sim \mathrm{O}(\epsilon)$ or less we have $\beta \sim \mathrm{O}(\epsilon^2) \ll 1$, which contradicts the above, and our task is complete. For general $\tau > 0$, note that the above reasoning means that we do need not to consider $1 \gg \beta > 0$, so without loss of generality, we can just consider $\beta \sim \mathrm{O}(\epsilon)$ *or greater*.

Therefore

$$\frac{\sin(\beta\tau)}{\beta\tau} = -\frac{1+\epsilon^2}{q_{22}\tau} + \mathrm{O}\left(\frac{\epsilon^2}{\beta q_{22}\tau}\right) = -\frac{1}{q_{22}\tau}(1+\mathrm{O}(\epsilon)) \tag{A.5}$$

and thus, $\pi < |\beta\tau| < q_{22}\tau(1+\mathrm{O}(\epsilon))$ with

$$\cos(\beta\tau) = \pm\left[1-(\beta/q_{22})^2(1+\mathrm{O}(\epsilon))\right]^{1/2} < 1, \tag{A.6}$$

for an appropriate choice of sign. The final inequality arises as β is bound away from zero. For any value of β which solves Eq. (A.5), we have that β, and hence $B(\beta,\tau)$, is bounded as $\epsilon \to 0$, and hence

$$\begin{aligned}\gamma_1(\beta,\tau) &= \frac{2\pi^2\epsilon^2}{A(\beta\tau)+\sqrt{A^2(\beta\tau)-\epsilon^2 B(\beta,\tau)}} = \frac{\pi^2\epsilon^2}{A(\beta\tau)}(1+\mathrm{O}(\epsilon^2)) \\ &= \frac{\pi^2\epsilon^2}{p_{22}\pm q_{22}\sqrt{1-(\beta/q_{22})^2(1+\mathrm{O}(\epsilon))}}(1+\mathrm{O}(\epsilon^2)) \\ &> \frac{\pi^2\epsilon^2}{p_{22}+q_{22}}(1+\mathrm{O}(\epsilon^2)) = \gamma_1(0,\tau).\end{aligned}$$

The above inequality arises from (A.6), on noting that $q_{22} > 0$ and entails that the above value of $\gamma_1(\beta,\tau)$ cannot correspond to the bifurcation. All the above generalises if Eq. (A.4) is achieved via a combination of any of the above mentioned possibilities; for example $C(\beta,\tau) \sim \mathrm{O}(1/\epsilon)$ and $\left[\beta(1+\epsilon^2)+q_{22}\sin(\beta\tau)\right] \sim \mathrm{O}(\epsilon)$. Thus, we must have that $\beta = 0$ at the bifurcation point, and hence there is no oscillation.

A. 3.2 Derivation of Eq. (6)

Once more, let $p_{11}, p_{12}, \ldots, q_{21}, q_{22}$ denote the components of **P** and **Q** in Eq. (9). For no time delay, i.e. $\tau = 0$, with $\delta \geq 0$, substitute Eq. (5) into Eq. (4). This again yields Eqs. (A.1) to (A.3), though now for $\tau = 0,\ \delta \geq 0$. The results derived in the previous section generalise immediately, and thus we have $\beta = 0$ and $n = 1$ at the bifurcation point in the absence of a time delay. Hence, substituting $\tau = 0, \beta = 0, n = 1$ into Eq. (A.1), with $\delta \geq 0$, yields Eq. (6).

Instead suppose $\tau \geq 0,\ \delta = 0$. From the previous section we have $\beta = 0$ at the bifurcation point. Furthermore we have γ_{crit} is given by Eq. (A.1) and, by inspection of Eq. (A.3), we have that $A(0)$ and $B(\beta = 0,\tau)$ are independent of τ. Thus, Eq. (6), which is valid for $\delta = \tau = 0$, from above, is also valid for $\delta = 0,\ \tau > 0$.

A. 4 Comparison of linear theory large time asymptotes and non-linear theory

For $\epsilon^2 = 0.001$, it is interesting to note that the large time asymptotes of the linear system given by Eq. (9) are O(1) or not according to whether $\tau\delta$ is greater or less than 0.057; see Appendix A.1. However, detailed non-linear numerical simulations (not shown) demonstrate that the Turing instability will always occur once

$\tau\delta < 0.084$ when $\epsilon^2 = 0.001$. Thus, in the region $\tau\delta \in [0.057, 0.084]$ there is distinct disagreement between the behaviour of the linear theory's large time asymptotes and the non-linear simulations. This is presumably because although within this region the linear theory predicts initial perturbations should eventually decay at large time, the intermediate growth is sufficient to trigger non-linearities in the equations and effect a Turing instability. We may conclude that even the large time asymptotes of the linear theory are not particularly accurate predictors for the behaviour of the full non-linear equations, though they indicate the correct order of magnitude for the critical value of $\tau\delta$ concerning the onset of a Turing instability.

B Additional details

B.1 Algebraic expressions for the initial conditions

The algebraic expressions for $a_{\mathrm{IC}=1}(x)$, $b_{\mathrm{IC}=1}(x)$, as plotted in Fig. 2, are

$$\begin{aligned} a_{\mathrm{IC}=1}(x) &= 0.9 + E_a x^5(1-x^2)[A_a x^3 + B_a x^2 + C_a x + D_a], \\ b_{\mathrm{IC}=1}(x) &= 1.0 - E_b x^7(1-x^2)[A_b x^3 + B_b x^2 + C_b x + D_b], \end{aligned} \tag{B.1}$$

with $x \in [0, 1]$, where $E_a = 0.00125$, $E_b = 0.00600$ and

$$A_a = -170.6666682, \quad B_a = 412.4444479, \quad C_a = -312.8888910, \quad D_a = 71.1111113,$$
$$A_b = -130.8444445, \quad B_b = 337.0666669, \quad C_b = -281.6000002, \quad D_b = 75.3777778.$$

The substantial accuracy for the quoted values of $A_a, B_a, \ldots, D_b$ are so that the perturbations remain small in the interval $x \in [0, 1]$ and, especially, that they satisfy the zero flux boundary conditions. They are not indicative of the conclusions

Table B.1 A reference set of parameter estimates for Eq. (8), used for Fig. (7). The final time T is such that the domain length increases by a factor of 70 (2SF) during the run. As previously, the timescale is taken to be $1/\lambda$.

Parameter	Value
Diffusivity of the inhibitor (D, $\mathrm{cm^2\,s^{-1}}$)	10^{-6}
Decay rate of the activator (λ, $\mathrm{min^{-1}}$)	1/3.1
Rate of exponential domain growth ($\delta = \dot{\gamma}/\gamma$)	0.000375
Non-dimensionalised base rate production	
Inhibitor (p)	0.90
Activator (q)	0.10
Ratio of diffusion coefficient (ϵ^2)	0.016
Ratio of gene expression time delay to representative small time delay (τ/τ_0)	$\tau/\tau_0 \in \{0.0, 1.0, 2.0, 4.0, 8.0, 16.0\}$
Time (t)	$t \in [0, T = 2266]$
Representative small time delay (τ_0, min)	3.875
Initial value of γ ($\gamma(t = 0)$)	5.0×10^{-3}

Table B.2 A reference set of parameter estimates for Eq. (8), used for Fig. (8). The final time is T is such that the domain length increases by a factor of 70 (2SF) during the run. As previously, the timescale is taken to be $1/\lambda$.

Parameter	Value
Diffusivity of the inhibitor (D, $\mathrm{cm}^2\,\mathrm{s}^{-1}$)	10^{-6}
Decay rate of the activator (λ, min^{-1})	1/3.1
Rate of exponential domain growth ($\delta = \dot{\gamma}/\gamma$)	0.0060
Non-dimensionalised base rate production	
Inhibitor (p)	0.90
Activator (q)	0.10
Ratio of diffusion coefficient (ϵ^2)	0.016
Ratio of gene expression time delay to representative small time delay (τ/τ_0)	$\tau/\tau_0 \in \{0.0, 1.0, 2.0, 4.0, 8.0, 16.0\}$
Time (t)	$t \in [0, T = 1416]$
Representative small time delay (τ_0, min)	3.875
Initial value of γ ($\gamma(t = 0)$)	5.0×10^{-3}

of this paper requiring an extreme fine tuning of the initial conditions. We further discuss issues associated with robustness in Sections 5.1 and 5.2.1.

B.2 Table of the variables and parameters used in the main text

Variable/ parameter	Definition/interpretation	First defined
$a_{\mathrm{IC}=1}(x)$	Functions used to construct representative initial conditions. Similarly for $a_{IC=2}(x)$, $b_{IC=2}(x)$, $b_{\mathrm{IC}=1}(x)$.	Section 3.2
a, b	Inhibitor and activator concentrations, respectively.	Section 2.1
a_*, b_*	Levels of inhibitor, activator at the homogeneous steady state.	Section 2.1.1
$\mathbf{A}_n(t)$	Time dependence of the n^{th} mode in a linear analysis.	Section 2.1.1
D	Diffusion coefficient of the inhibitor (dimensional).	Section 2.1
IC	Initial condition label; see figure captions and Section (3.2).	Section 3.2
L, L_0	Dimensional domain length.	Section 2.1
p, q	Non-dimensionalised base rate production of inhibitor and activator, respectively.	Section 2.1
$\mathbf{P}$, $\mathbf{Q}$	Matrices in time delayed linearised equations.	Section 2.2.1
t	Time.	Section 2.1
T_{del}	$T_{\mathrm{del}} = \tau/\tau_0$; see figure captions for details.	Figure 3
T	T is the final time of the simulations in Tables 1-B.2.	Table 1
u	Domain growth velocity field.	Section 2.2
x	$x \in [0, 1]$ is the normalised spatial coordinate	Section 2.1
y	Spatial coordinate on the physical domain.	Section 2.2
y_τ	$y_\tau = Y_y(s = t - \tau)$.	Section 2.2

Variable/ parameter	Definition/interpretation	First defined
$Y_y(s)$	Solution of $dY_y/ds = u(Y, s)$ with $Y_y(s = t) = y$. It traces a material point in the moving domain.	Section 2.2
$\gamma, \gamma(t)$	$\gamma = \lambda L^2/D, \quad \gamma(t) = \lambda L^2(t)/D = \lambda L_0^2 \exp(\delta t)/D.$	Section 2.1
γ_0	γ_0 is defined to be $\gamma(t = 0)$	Figure 4
γ_{crit}	Value of γ for which $Re(\lambda_n)$, $n \in \mathbb{Z}^+$, first becomes non-negative on increasing γ from a sufficiently small value.	Section 2.1.1
δ	$\delta = \dot{\gamma}/\gamma$; δ governs the rate of exponential domain growth.	Section 2.1
ϵ^2	The ratio of the activator diffusion coefficient to the inhibitor diffusion coefficient.	Section 2.1
η	Size of perturbations in the linear analyses.	Section 2.1.1
λ	Decay rate of activator given no domain growth (dimensional).	Section 2.1
λ_n	Exponential growth rate of the n^{th} mode in a linear analysis.	Section 2.1.1
τ	Gene expression time delay.	Section 2.2
τ_0	A representative small time delay, as defined in Table 1.	Table 1

Acknowledgements

It is a pleasure for EAG to acknowledge useful discussions with Dr. Fordyce Davidson concerning time delays.

References

Arcuri, P., Murray, J.D., 1986. Pattern sensitivity to boundary and initial conditions in reaction diffusion models. J. Math. Biol. 24, 141–165.

Bard, J., Lauder, I., 1974. How well does Turing's theory of morphogenesis work? J. Theor. Biol. 45, 501–531.

Boushaba, K., Ruan, S., 2001. Instability in diffusive ecological models with non-local delay effects. J. Math. Anal. Appl. 258, 269–286.

Branford, W.W., Yost, H.J., 2002. Lefty-dependent antagonism of the Nodal and Wnt signalling pathways is essential for normal gastrulation. Curr. Biol. 12, 2136–2141.

Branford, W.W., Yost, H.J., 2004. Nodal signalling: Cryptic lefty mechanism of antagonism decoded. Curr.nt Biol. 14, R341–R343.

Bunow, B., Kernevez, J.P., Joly Thomas, G., 1980. Pattern formation by reaction-diffusion instabilities: Applications to morphogenesis in *Drosophila*. J. Theor. Biol. 84, 629–649.

Chen, C., Shen, M.M., 2004. Two modes by which lefty proteins inhibit nodal signalling. Curr. Biol. 14, 618–624.

Chen, Y., Schier, A.F., 2001. The zebrafish Nodal signal Squint functions as a morphogen. Nature 411, 607–610.

Chen, Y., Schier, A.F., 2002. Lefty proteins are long-range inhibitors of Squint-mediated Nodal signalling. Curr. Biol. 12, 2124–2128.

Crampin, E.J., Gaffney, E.A., Maini, P.K., 1999. Reaction and diffusion on growing domains: Scenarios for robust pattern formation. Bull. Math. Biol. 61, 1093–1120.
Crampin, E.J., Gaffney, E.A., Maini, P.K., 2002. Mode-doubling and tripling in reaction-diffusion patterns on growing domains: A piecewise linear model. J. Math. Biol. 44, 107–128.
Glimm, T., Glazier, J.A., Newman, S.A., 2004. Dynamical mechanisms for skeletal pattern formation in the vertebrate limb, HGE Hentschel. Proc. R. Soc. Lond. B 271, 1713-1722.
Goodwin, B.C., Murray, J.D., Baldwin, D., 1985. Calcium: The elusive morphogen in *Acetabularia*. In: Bonnotto, S., Cinelli, F., Billiau, R. (Ed.), Proceedings 6th International Symposium on *Acetabularia*, Pisa, Belgium, 1984. Belgian Nuclear Centre, CEN-SEK Mol, Belgium, pp. 101–108.
Gourley, S.A., Ruan, S., 2002. Spatio-temporal delays in a nutrient-plankton model on a finite domain: Linear stability and bifurcations. Appl. Math. Comput. 145, 391–412.
Jung, H.S., Francis-West, P.H., Widelitz, R.B., Jiang, T., Ting-Berreth, S., Tickle, C., Wolpert, L., Chuong, C., 1998. Local inhibitory action of BMPs and their relationships with activators in feather formation: Implications for periodic patterning. Dev. Biol. 196, 11–23.
Kimmel, C.B., Ballard, W.W., Kimmel, S.R., Ullmann, B., Schilling, T.F., 1995. Stages of embryonic development of the zebrafish. Dev. Dyn. 203, 253–310. See also www.zfin.org/zf_info/zfbook/stages.
Kondo, S., Asai, R., 1995. A reaction-diffusion wave on the skin of Pomacanthus, the marine Angelfish. Nature 376, 765–768.
Lewis, J., 2003. Autoinhibition with transcriptional delay: A simple mechanism for the Zebrafish somitogenesis oscillator. Curr. Biol. 13, 1398–1408.
Li, Q.S., Ji, L., 2004. Control of Turing pattern formation by delayed feedback. Phys. Rev. E 69, 046205-1–046205-4.
Mahaffy, J.M., 1988. Genetic control models with diffusion and delays. Math. Biosci. 90, 519–533.
Mahaffy, J.M., Pao, C.V., 1984. Models of genetic control by repression with time delays and spatial effects. J. Math. Biol. 20, 39–57.
Meinhardt, H., 1982. Models of Biological Pattern Formations. Academic Press, New York.
Miura, T., Maini, P.K., 2004. Speed of pattern appearance in reaction-diffusion models: Implications in the pattern formation of limb bud mesenchyme cells. Bull. Math. Biol. 66, 627–649.
Miura, T., Shiota, K., 2000. Extracellular matrix environment influences chondrogenic pattern formation in limb bud micromass culture: Experimental verification of theoretical models. Anat. Rec. 258, 100–107.
Monk, N.A.M., 2003. Oscillatory expression of Hes1, p53, and NF-kappa B driven by transcriptional time delays. Curr. Biol. 13, 1409–1413.
Murray, J.D., 1981. A pre-pattern formation mechanism for animal coat markings. J. Theor. Biol. 88, 161–199.
Murray, J.D., 1993. Mathematical Biology. Springer-Verlag, Berlin.
Murray, J.D., Oster, G.F., Harris, A.K., 1983. A mechanical model for mesenchymal morphogenesis. J. Math. Biol. 17, 125–129.
Oster, G.F., Murray, J.D., Harris, A.K., 1983. Mechanical aspects of mesenchymal morphogenesis. J. Embryol. Exp. Morphol. 78, 83–125.
Ouyang, Q., Swinney, H.L., 1991. Transition from a uniform state to hexagonal and striped Turing patterns. Nature 352, 610–612.
Page, K.M., Maini, P.K., Monk, N.A.M., 2005. Complex pattern formation in reaction diffusion systems with spatially-varying parameters. Physica D 202, 95–115.
Ruan, S., 1998. Turing instability and travelling waves in diffusive plankton models with delayed nutrient recycling. IMA J. Appl. Math. 61, 15–32.
Solnica-Krezel, L., 2003. Vertebrate development: Taming the nodal waves. Curr. Biol. 13, R7–R9.
Tabata, T., Takei, Y., 2004. Morphogens, their identification and regulation. Development 131, 703–712.
Tennyson, C.N., Klamut, H.J., Worton, R.G., 1995. The human dystrophin gene requires 16 h to be transcribed and is cotranscriptionally spliced. Nat. Gen. 9, 184–190.
Turing, A., 1952. The chemical basis of morphogenesis. Phil. Trans. R. Soc. Lond. B237, 37–72.
Veflingstad, S.R., Plahte, E., Monk, N.A.M., 2005. Effect of time delay on pattern formation: Competition between homogenisation and patterning. Physica D 207, 254–271.
Vincent, J.P., Briscoe, J., 2001. Morphogens. Curr. Biol. 11, R851–R854.